



Additives for morphology control in high-efficiency organic solar cells

**Hsueh-Chung Liao¹, Chun-Chih Ho¹, Chun-Yu Chang¹, Meng-Huan Jao¹,
Seth B. Darling^{2,3,*} and Wei-Fang Su^{1,*}**

¹ Department of Materials Science and Engineering, National Taiwan University, Taipei 106-17, Taiwan

² Center for Nanoscale Materials, Argonne National Laboratory, 9700 South Cass Avenue, Argonne, IL 60439, USA

³ Institute for Molecular Engineering, University of Chicago, Chicago, IL 60637, USA

Bulk heterojunction (BHJ) photovoltaics represent one of the most promising technologies in low-cost, high-throughput, environmentally friendly energy conversion. Morphological control is one pillar of the recent remarkable progress in power conversion efficiency. This review focuses on morphological control by processing with solvent additives, which has been extensively adopted and exhibits promising compatibility with large-scale processing. Recent investigations including material selection, morphological variations at various length scales, and interpretations of the interaction among additives and BHJ materials will be discussed. Insights into the role of solvent additives represent an important resource for further improvement in materials and processing designs.

Introduction

Organic photovoltaics (OPVs) have experienced an explosive growth in investigations over the last two decades as an alternative photovoltaic (PV) to conventional systems based on inorganic semiconductors. The chemically tunable properties of organic materials in combination with high-throughput roll-to-roll solution processing make OPVs promising in providing low-cost and environmentally benign [104] energy conversion. Other advantages, including mechanical flexibility, light weight, and potential semi-transparency, reveal further potential applications of OPVs in a variety of commodity products, building construction, etc. Nevertheless, achieving true low cost relies on high power conversion efficiency (PCE), which is the main goal of recent investigations.

Lab-scale devices recently demonstrated significant advances in device performance with 8–9% certified PCEs in single-junction devices [2], and even higher efficiencies with tandem cells. A number of articles have comprehensively reviewed the crucial factors underlying such breakthroughs including materials development [3–5], morphology [6–10], device physics [11–13], device structure [14], etc. Among the factors, morphology plays one of

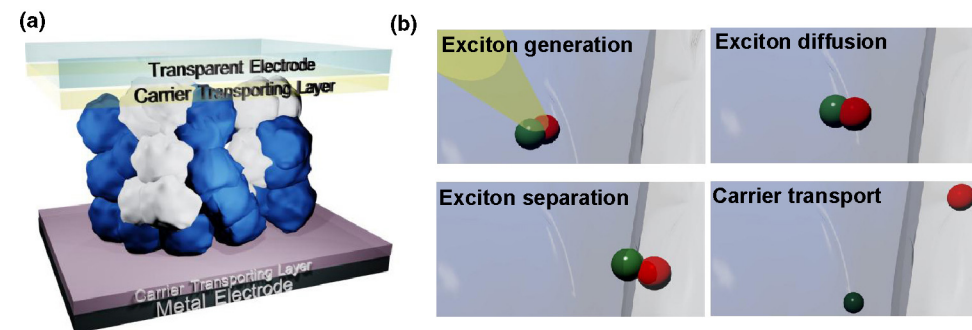
the most important roles in attaining high efficiency. An in-depth understanding of the interplay among processing, morphology, and optoelectronic properties is required for further improving the efficiency before OPVs can become competitive with inorganic PV systems.

Working mechanism of BHJ solar cells associated with nanomorphology

Bulk heterojunctions (BHJs), in which electron-donors and electron-acceptors are blended together (Fig. 1a), represent the most promising device structure for high-efficiency organic solar cells. The complex, three-dimensional nanostructures of BHJs have profound effects on the optoelectronic conversion efficiency; essentially all of the critical mechanisms of light-to-electricity conversion take place within the BHJ layer: (1) light harvesting and exciton generation, (2) exciton diffusion to a donor/acceptor interface, (3) exciton separation, and (4) carrier transport to the electrodes (Fig. 1b). Many papers [11,13,15] have reviewed these mechanisms in detail, thus herein we focus on the roles of nano- and/or mesoscale morphology as well as molecular ordering in each mechanism.

The absorption range and the capability of light harvesting of a BHJ layer are dominated by the molecular structure and electron

*Corresponding authors: Darling, S.B. (darling@anl.gov), Su, W.-F. (suwf@ntu.edu.tw)

**FIGURE 1**

(a) Illustration of typical BHJ device structure in which the phase-separated blending domains are sandwiched between carrier transporting layer/metal electrode and carrier transporting layer/transparent electrode. Note that the layers are not drawn to scale, rather, the active layer is expanded to schematically depict its morphology. (b) Illustrations of working mechanism of BHJ blends including exciton generation upon light excitation, exciton diffusion toward the donor/acceptor interface, exciton separation at the donor/acceptor interface, and carrier transport toward respective electrodes.

conjugation (coupling) of organic materials. The recent development of so-called push–pull or donor–acceptor type conjugated copolymers has resulted in tremendous success in rearrangement of energy levels and thus optical bandgap and absorption toward longer wavelengths [3–5]. Nevertheless, it is noteworthy that there are still close connections between light harvesting and BHJ nanomorphology, for example, influence of molecular ordering on intermolecular interaction and electron conjugation. Therefore, when studying processing effects on the nanomorphology, one should keep in mind that variations of light harvesting properties resulting from morphological changes should be taken into account with associated photovoltaic properties.

Upon light harvesting, a singlet exciton, comprising an electron and a hole bound together by the attractive Coulomb interaction, is generated (Fig. 1b) through photo-excitation. Organic materials generally exhibit relatively low dielectric permittivity of 3–4, which leads to weak screening and thus large exciton binding energy (hundreds of meV) that cannot be dissociated by ambient thermal energy (~ 0.025 eV at 298 K). Therefore, in order to dissociate the excitons, they must migrate toward the donor/acceptor interfaces where the built-in electric field, analogous to type II alignment in p–n junctions, provides driving force to separate the excitons. Generally, the average migration distance of excitons in organic materials ranges from 5 to 20 nm [16]. It can be imagined that if the phases of donor and acceptor possess large-scale segregation into pure phases (over tens or hundreds of nanometers), the singlet exciton would undergo geminate recombination prior to encountering the donor/acceptor heterojunction for dissociation.

As the excitons reach donor/acceptor interfaces, they undergo either ultrafast quenching to free polarons or conversion to charge transfer (CT) complexes. The CT states can be either detrimental or beneficial for early-time free carrier generation depending on their tendency to further evolve into free polarons [1]. For the latter case of CT complexes mediating exciton dissociation, CT complex separation competes with the process of geminate recombination. Specifically, the electron and hole must achieve a certain separation distance that is large enough to overcome their mutual Coulomb attractive force. From a morphological point of view, nanostructures adjacent to the interfaces are therefore critical, for example, locally high mobility and a molecular dipole or multipole offsetting the attractive force are expected to improve escape

efficiency of electrons and holes from the interface and thus the yield of useful carriers.

Following exciton dissociation, free electrons and holes diffuse or drift toward their respective electrodes through the acceptor-rich phase and donor-rich phase, respectively, to generate power. A high efficiency of free carriers being extracted by electrodes depends on bi-continuous transport routes of properly phase-separated donor and acceptor domains. A discontinuous pathway may result in inefficient means of transport such as inter-domain hopping and thus dramatically increases the opportunities of non-germinate recombination, a deleterious process in which carriers encounter opposite free carriers during transport.

State-of-the-art OPVs

The mechanisms described above affect the photovoltaic properties in terms of open circuit voltage (V_{OC}), short circuit current density (J_{SC}), and fill factor (FF), which can be determined by the measurement of the photocurrent density–voltage (J – V) curve. The PCE can be represented by the combination of these terms as expressed in Eqn 1:

$$\text{PCE} = \frac{V_{OC} \times J_{SC} \times FF}{P_{in}} \quad (1)$$

where P_{in} is incident light intensity. Additionally, the BHJ solar cell is typically implemented into a layered device structure in which the BHJ layer is sandwiched between carrier transporting layers buffering work functions and improving carrier collection between the BHJ active layer and the electrodes as shown in Fig. 1a. Herein we summarize the state-of-the-art of morphology controlled BHJ solar cells with PCE > 7% as listed in Table 1.

Processing and morphology of BHJs

The central role of morphology in essentially every aspect the photovoltaic process and device properties was emphasized in the *Working mechanism of BHJ solar cells associated with nanomorphology* section. Accordingly, a general picture of an idealized morphology would entail structure at various length scales: from local molecular ordering to global phase-separated domains or networks. However, simply solution processing the BHJ layer from a blend solution of donor material and acceptor material in a single solvent usually results in a morphology correlated with poor

TABLE 1

Morphology controlled BHJ polymer solar cells with PCEs >7%.

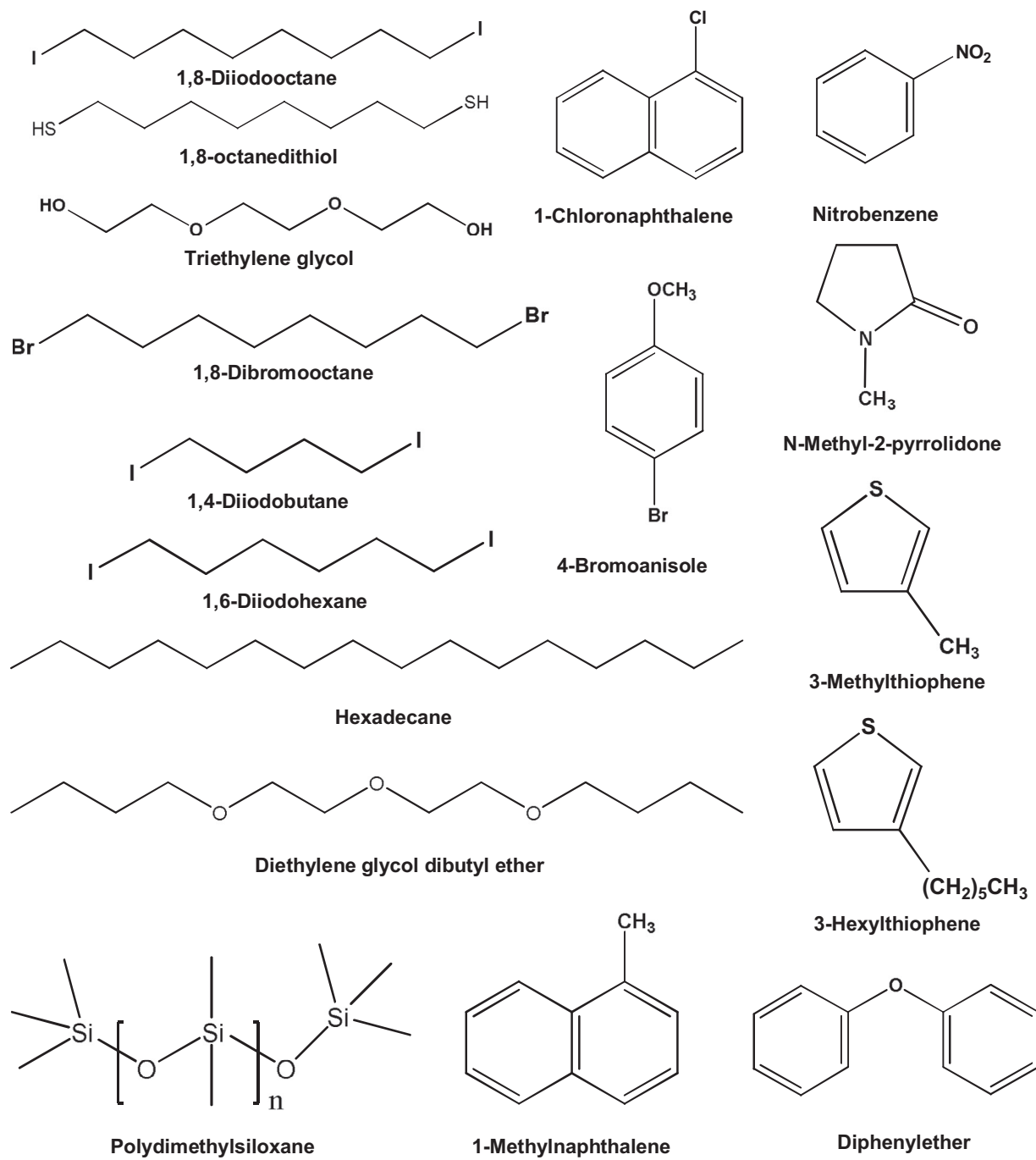
BHJ materials	PCE (%)	Strategy of BHJ morphology control	Ref.
Single junction device			
PTB7/PC ₇₁ BM	7.4–9.2	Processing with solvent additive	He [77] Zhou [78] Yoon [79] He [53] Liang [68]
PBDTTT-C-T/PC ₇₁ BM	7.6–8.8	Processing with solvent additive	Hou [80] Li [81]
PDTG-TPD/PC ₇₁ BM	7.3–8.5	Processing with solvent additive	Chen [82] Amb [83] Small [84]
PBDTTPD/PC ₇₁ BM	7.1–8.5	Processing with solvent additive or without treatment	Aich [85] Hoke [86] Cabanetos [87]
PBDT-DTNT/PC ₇₁ BM	8.4	Thermal annealing	Yang [88]
PDTP-DFBT/PC ₇₁ BM	7.9	None	You [2]
PBDTTT-CF/PC ₇₁ BA	7.7	Processing with solvent additive	Chen [89]
PIDT-PhanQ/PC ₇₁ BM	7.5	Thermal annealing	Yang [90]
P3HT/IC ₇₁ BA	7.4	Processing with solvent additive and thermal annealing	Guo [50]
PBDTTT-C/PC ₇₁ BA	7.4	Processing with solvent additive	Tan [91]
PBTTPD/PC ₇₁ BM	7.3	Processing with solvent additive	Su [73]
PDTSTPD/PC ₇₁ BM	7.3	Processing with solvent additive	Chu [92]
P3HT/IC ₆₁ BA	7.3	Thermal annealing	Chang [93]
PBnDT-DTffBT/PC ₆₁ BM	7.2	None	Zhou [94]
PBnDT-FTAZ/PC ₆₁ BM	7.1	None	Price [95]
DTffBT/DTPyT/PC ₆₁ BM	7.0	None	Yang [96]
PFDCBT-BT-C8/PC ₇₁ BM	7.0	Thermal annealing	Chang [97]
PMDPP3T/PC ₇₁ BM	7.0	Processing with solvent additive	Li [38]
PT small molecules/PC ₇₁ BM	7.0	Processing with solvent additive	Takacs [98]
Multi-junction device			
Front: P3HT/IC ₆₁ BA Rear: PDTP-DFBT/PC ₆₁ BM	10.6	Front: Thermal annealing Rear: None	You [2]
First: PCDTBT/PC ₇₁ BM Second: PMDPP3T/PC ₇₁ BM Third: PMDPP3T/PC ₇₁ BM	9.6	First: Thermal annealing Second: Processing with solvent additive Third: Processing with solvent additive	Li [38]
Front: P3HT/IC ₆₁ BA Rear: PBDTT-DPP/PC ₇₁ BM	8.6–8.8	Front: Thermal annealing Rear: None	Dou [99,100]
Front: P3HT/IC ₆₁ BA Rear: PSBTBT:PC 70 BM	7.0	Front: Thermal annealing Rear: Thermal annealing	Yang [101]
Front: PCDTBT/PC ₇₁ BM Rear: PDPP5T/PC ₆₁ BM	7.0	Front: Thermal annealing Rear: Processing with solvent additive	Gevaerts [39]

performance. Therefore, methodologies to obtain a favorable morphology by adjustments to processing have been extensively investigated, for example, thermal annealing [17–20], solvent vapor annealing [18,21], using additives including small molecules [22,23], polymers [24–28], inorganic nanocrystals [29], high boiling solvents (cf. Table 1), etc. Among the strategies, processing with solvent additive in addition to the primary host solvent – an approach developed in the mid-2000s [30–32] – has been found widely effective for BHJ morphology control and compatible with large-scale processing [33,34]. A collection of high-efficiency solar cells adopting this strategy are summarized in Table 1. In this review, we focus on this technique, starting from the intrinsic properties and exploring the criteria for solvent additives. Recent investigations on BHJ morphological variations at various length scales affected by solvent additives will be reviewed. Furthermore, studies focusing on structural evolution will also be covered to provide insights into the interaction among BHJ blending

materials, host solvents, and additives during processing. It is our expectation that this review can provide the groundwork to rationally guide further materials and processing designs.

Morphological control by solvent additives*Materials*

Generally, there are two central guidelines in selecting host solvent and additives [35]: (1) host solvents usually possess high solubility to both electron donor and acceptor molecules whereas solvent additives have selective solubility to one of the components (typically the acceptor), and (2) solvent additives are typically less volatile with higher boiling points than host solvents. Following the guidelines mentioned above, various kinds of solvent additive molecules have been incorporated in BHJ processing, which are illustrated in Fig. 2. A key point is that the role of solvents can be varied depending on their interaction with donor materials and acceptor materials, respectively. For example,

**FIGURE 2**

Examples of solvent additives for BHJ morphological control.

ortho-dichlorobenzene (*o*-DCB) in most cases is an excellent host solvent with high solubility for conjugated semiconductors; however, the work reported by Liu et al. [36] and Wienk et al. [37] demonstrated that the copolymer of diketopyrrolopyrrole and quaterthiophene (pDPP) is poorly dissolved in *o*-DCB but well dissolved in chloroform (CF). Therefore, during processing of such copolymer/fullerene BHJ blends, the *o*-DCB in the co-solvent *o*-DCB/CF functions as a solvent additive because of its selective solubility to fullerene and higher boiling point than CF – a situation that may be analogously applicable in other BHJ systems [38,39].

Quantifying and/or predicting the solubility of a given solvent to the BHJ components is invaluable for guiding proper selection of solvents and solvent additives. A preliminary screening can be achieved by calculating the Hansen solubility [40] parameters of polymers, oligomer, or small molecules as recently applied by Graham et al. [41], Walker et al. [42], and Duong et al. [43]. The Hansen solubility parameters in terms of dispersion (δ_D), polarity (δ_P), and hydrogen bonding (δ_H) were derived from the cohesive energy density (CED) parameters, which had been used to evaluate solvent quality [44]. After calculating the values of each

term for two substances respectively, the Hansen solubility space, R_a , can be calculated by Eqn 2 [40]

$$R_a = \sqrt{4(\delta_{D2} - \delta_{D1})^2 + (\delta_{P2} - \delta_{P1})^2 + (\delta_{H2} - \delta_{H1})^2} \quad (2)$$

where the subscripts 1 and 2 indicate the parameters of the two substances, respectively. The value of R_a can be used to imply the favorability between two substances, for example, miscibility, solubility, tendency of phase separation, etc. Although these parameters ignore several factors such as $\pi-\pi$ stacking and crystal structures, this approximation can be still serve as an index to compare the relative solubility of a solvent either to donor or acceptor materials and narrow down the selection range of processing solvents.

Experimentally, the solubility can be quantified by loading sufficient amounts of solutes into the solvents and separating

the dissolved and un-dissolved parts by centrifugation or filtration [41,42]. An alternative approach was reported by Liu et al., who measured swelling isotherms by exposing the deposited organic films to an environment filled with various solvent vapor pressures and tracking the differences of optical absorption [45]. Accordingly, the swelling threshold of organic materials by solvent vapor can be extracted and correlated to the Flory-Huggins interaction parameter χ .

Molecular organization

To begin a discussion on the effects of processing additive on BHJ morphology, we start with the local scale of molecular ordering with particular interest in crystalline nanostructures including crystallinity, crystal orientation, crystal size, and inter-layer spacing. Reciprocal space techniques such as wide angle X-ray

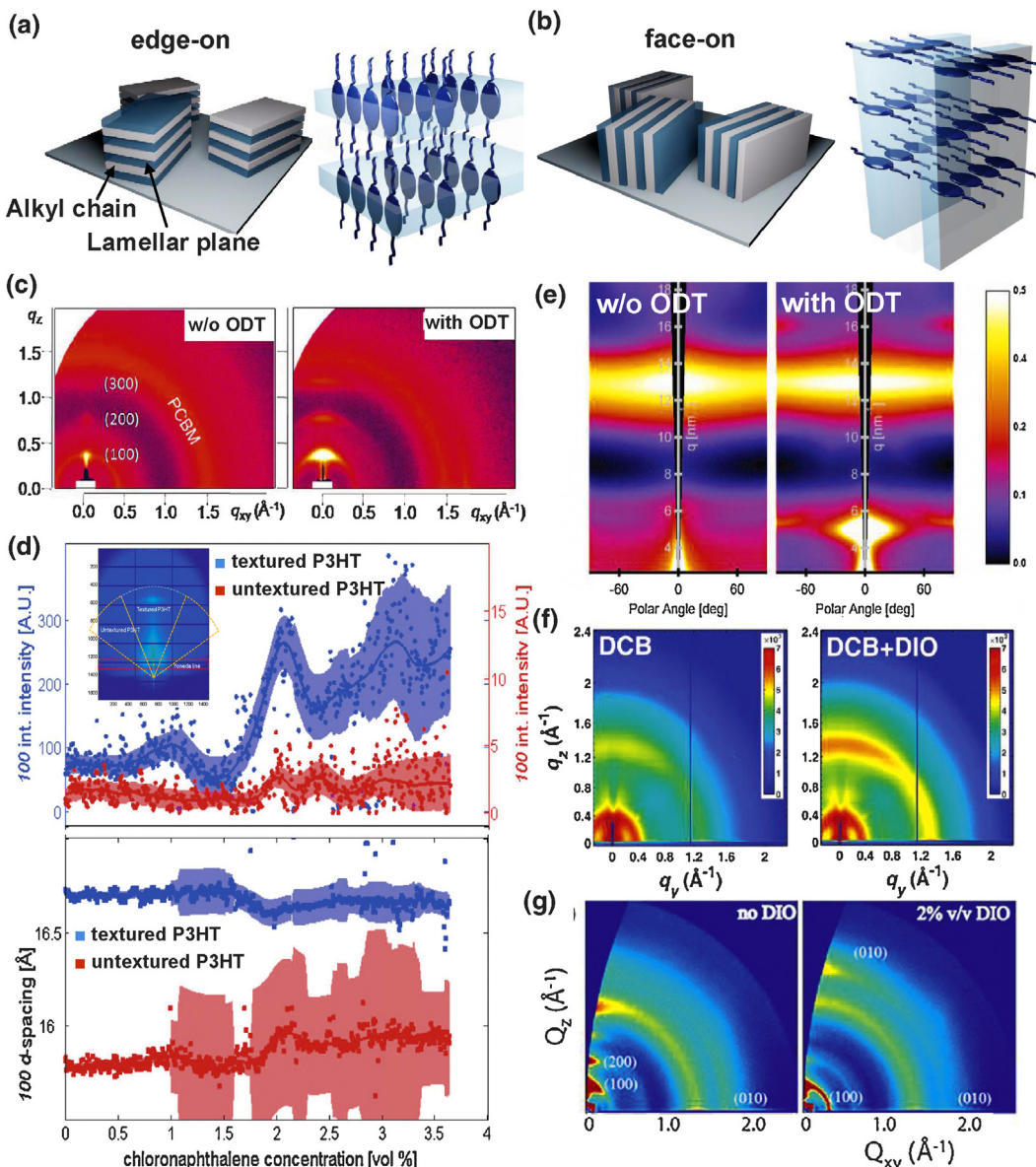


FIGURE 3

(a and b) Illustrations of face-on and edge-on crystallites. (c–g) Characterization of molecular ordering in BHJ films processed without/with solvent additives. (c) 2D GIWAXS patterns of P3HT/PC₆₁BM BHJ. (d) Structural parameters of (100) plane of P3HT/PC₆₁BM BHJ with various additive concentrations. (e) 2D GIWAXS sector plots of PCPDTBT/PC₇₁BM BHJ. (f) 2D GIWAXS patterns of PTB7/PC₇₁BM BHJ. (g) 2-D GIAXS patterns of PII2T-Si/PC₇₁BM BHJ. Reproduced with permission from [46,47,51,54,57]. © American Chemical Society, © Royal society, © Wiley.

scattering (WAXS) provide powerful information on short-range order, including the possibility for quantitative characterization of orientation through the assistance of a two-dimensional (2D) detector.

The most widely studied homopolymer/fullerene BHJ is a poly(3-hexylthiophene-2,5-diyl)/[6,6]-phenyl-C₆₁-butyric acid methyl ester (P3HT/PC₆₁BM) blend. In this system, the P3HT chains tend to organize into lamellar crystalline structures preferentially parallel to the substrate (i.e. edge-on crystallites with hexyl side chains and polymer backbones perpendicular and parallel to the substrate, respectively) as depicted in Fig. 3a,b. The edge-on crystallites contribute to strong diffraction from the (1 0 0) lamellar plane in the out-of-plane direction (q_z) as illustrated in the grazing incidence WAXS (GIWAXS) pattern in Fig. 3c [46]. A BHJ film processed with the additive octanedithiol (ODT) resulted in a more intense (1 0 0) diffraction spot as compared to that processed without additive. This result reveals the effect of solvent additive on enhancing the crystallinity, which is similarly dominated by edge-on crystallites (though with a subtly tilted angle as seen in the texture of the diffraction spot). Enhanced crystallinity can be attributed to either an increased number of crystallites or larger crystal size. The latter structural parameter of crystal size (L) can be estimated by the Scherrer equation $L = 2\pi/\Delta q$, where Δq is the full width at half maximum (FWHM) of the diffraction peak. Following this analysis, larger crystal size was found in additive-processed BHJs [46–48]. Additionally, for the edge-on crystallites, the lamellar spacing d is also critical due to its indication of the packing along the vertical direction, which is the direction of

carrier transport. Processing with additive led to a shift of the diffraction peak position toward a higher diffraction angle, implying contraction of the lamellar spacing according to the relation $d_{(h k l)} = 2\pi/q_{(h k l)}$ [46]. Similar results of better packed lamellar structures were demonstrated by Böttiger et al. using roll-to-roll X-ray characterization of additive concentration (Fig. 3d) [47] and in another similar BHJ blend of P3HT/indene-C₇₀bisadduct (IC₇₀BA) [49]. It is noteworthy that an opposite effect of solvent additive on crystallinity was recently reported by Guo et al. in the same P3HT/IC₇₀BA BHJ [50]. The reason for the observed reduced P3HT crystallinity when prepared with additive was not clear; however, it is generally believed that the degree of crystallization of P3HT is positively correlated with device performance.

Regarding BHJs based on newer, donor–acceptor type conjugated copolymer, the effects of additive on the crystal structure can be distinctive among different BHJ systems. For one of the model BHJs: poly[2,6-(4,4-bis(2-ethylhexyl)-4H-cyclopenta[2,1-b;3,4-b']-dithiophene)-alt-4,7-(2,1,3-benzothiadiazole)]/[6,6]-phenyl C₇₁-butyric acid methyl ester (PCPDTBT/PC₇₁BM) processed with the additive diiodooctane (DIO), similar enhancement of crystallinity dominated by edge-on crystallites were found by Rogers et al. [51,52]. The GIWAXS sector plots of such a BHJ processed with DIO (Fig. 3e) show two types of crystallites with different lamellar spacing of (1) 1.26 nm, showing strong (1 0 0) (alkyl chain stacking) and (0 1 0) (π – π stacking) diffraction in out-of-plane $q_z = 5.1 \text{ nm}^{-1}$ and in-plane $q_{xy} = 16.2 \text{ nm}^{-1}$, respectively, and (2) 1.14 nm with (1 0 0) diffraction in out-of-plane $q_z = 5.5 \text{ nm}^{-1}$. More in-depth information on the crystal orientation was quanti-

TABLE 2

Effects of solvent additive on crystalline nanostructure of in various BHJ system.

BHJ materials	Additive	Crystallinity	Interlayer spacing, $d_{(h k l)}$	Crystal size	Ref.
P3HT/PC ₆₁ BM	Octanedithiol	Increase	Decrease ($d_{(1 0 0)}$ of edge-on type)	Increase	Chen [46]
P3HT/PC ₆₁ BM	Chloronaphthalene	Increase	Decrease ($d_{(1 0 0)}$ of edge-on type)	Increase	Böttiger [47]
P3HT/PC ₆₁ BM	Methylthiophene	Increase	Decrease (average $d_{(1 0 0)}$)	Increase	Salim [48]
	Hexylthiophene				
	Octanedithiol				
	Nananedithiol				
P3HT/IC ₇₀ BA	Methylthiophene	Increase	Decrease (average $d_{(1 0 0)}$)	N/A	Sun [49]
P3HT/IC ₇₀ BA	Hexylthiophene				
P3HT/IC ₇₀ BA	Diiodooctane	Decrease	N/A	N/A	Guo [50]
	Chloronaphthalene				
	N-methyl pyrrolidone				
	Octanedithiol				
PCPDTBT/PC ₇₁ BM	Diiodooctane	Increase	N/A ^a	N/A ^a	Gu [76]
	Octanedithiol				
	Dichlorooctane				
PCPDTBT/PC ₇₁ BM	Octanedithiol	Increase	N/A ^a	N/A ^a	Rogers [51,52]
PTB7/PC ₇₁ BM	Diiodooctane	Increase	No change ($d_{(1 0 0)}$ of face-on type)	No change	Chen [54]
			No change ($d_{(0 1 0)}$ of face-on type)		
PTB7/PC ₇₁ BM	Diiodooctane	No change	No change (average $d_{(1 0 0)}$)	No change	Hammond [55]
PTB7/PC ₇₁ BM	Diiodooctane	No change	No change (average $d_{(0 1 0)}$)	No change	Collins [56]
PII2T-Si/PC ₇₁ BM	Diiodooctane	Increase	Increase (average $d_{(1 0 0)}$)	N/A	Kim [57]
PBTPD/PC ₇₁ BM	Diiodobutane	Increase	N/A	Increase (face-on type)	Su [73]
	Diiodohexane			Decrease (edge-on type)	
	Diiodooctane				
TQ1/PC ₇₁ BM	Chloronaphthalene	Increase	Increase (average $d_{(1 0 0)}$)	N/A	Kim [102]
TBD-based/PC ₆₁ BM	Diiodooctane	Increase	Decrease (average $d_{(0 1 0)}$)	No change	Piliego [103]
PDPP3T/PC ₇₁ BM	Diiodooctane	Increase	N/A	Increase	Ye [60]

^a The BHJ processed without additives shows amorphous polymeric morphology with no diffraction peaks.

tatively characterized by the index of orientational order S to illustrate the orientational evolution of type (1) and type (2) crystallites toward more and lesser edge-on orientation during additive drying [52]. Subsequently, extensive investigations were devoted to the thieno[3,4-b]thiophene-*alt*-benzodithiophene based copolymer (PTB7)/PC₇₁BM, which holds the current record PCE in a single junction device [53]. As shown in Fig. 3f, this BHJ features a crystalline structure dominated by face-on crystallites (Fig. 3b), which is considered to be beneficial for carrier transport [54–56]. Because of this orientation, interest in the interlayer spacing shifts to the π - π stacking, that is, spacing of (0 1 0) planes, along the vertical direction. While the crystallinity is analogously intensified by the additive DIO, no significant changes of (0 1 0) spacing, crystal size, or crystal orientation were observed when processed with additive [54]. However, overall crystallinity does increase with addition of DIO, suggesting the presence of a larger number of crystallites of similar size [54]. Note that the crystal orientation is not always insensitive to additives as the BHJ systems mentioned above. A study by Kim et al. [57] reported dramatic change of orientation distribution from edge-on crystallites to randomly oriented crystallites in a BHJ system based on an isoindigo polymer (PII2T-Si/PC₇₁BM) (Fig. 3g).

We can generally conclude the low vapor pressure solvent additive has a pronounced effect of enhancing crystallinity in most BHJs, though the detailed variation of crystallization behavior regarding the crystal size, number of crystallites, interlayer

spacing, and crystal orientation depends on the specific BHJ system under study. We summarize the processing additive effects on crystalline structures in various BHJ systems with respect to the crystallinity, crystal size, and interlayer spacing in Table 2. It is noteworthy that higher crystallinity had been the typical target during processing because of the high carrier mobility and strong inter-molecular interaction (stronger light absorption) in ordered molecular systems [58,59]. Demonstrating the complexity of this topic, however, recent developments of high-efficiency solar cells evidenced only a minor effect of crystallinity on device performance in some BHJ systems [55,56,60]. It is hence difficult to generalize the correlation between crystallinity and photovoltaic properties among various BHJ systems. One point that is generally true regarding crystallinity is that the amount of available interfacial area between donors and acceptors may also play an important role in the performance of polymer solar cells [61].

Phase-separated domains

Additive effects on larger length scales, tens or hundreds of nanometers, are significant and regarded as a major factor accounting for the dramatically improved PCEs associated with their use. Recent progress with characterization techniques in microscopic observations, for example, transmission electron microscope (TEM), atomic force microscope (AFM), etc., and reciprocal-space techniques, for example, small angle X-ray/neutron scattering (SAXS/SANS) enables complementary and quantitative structural

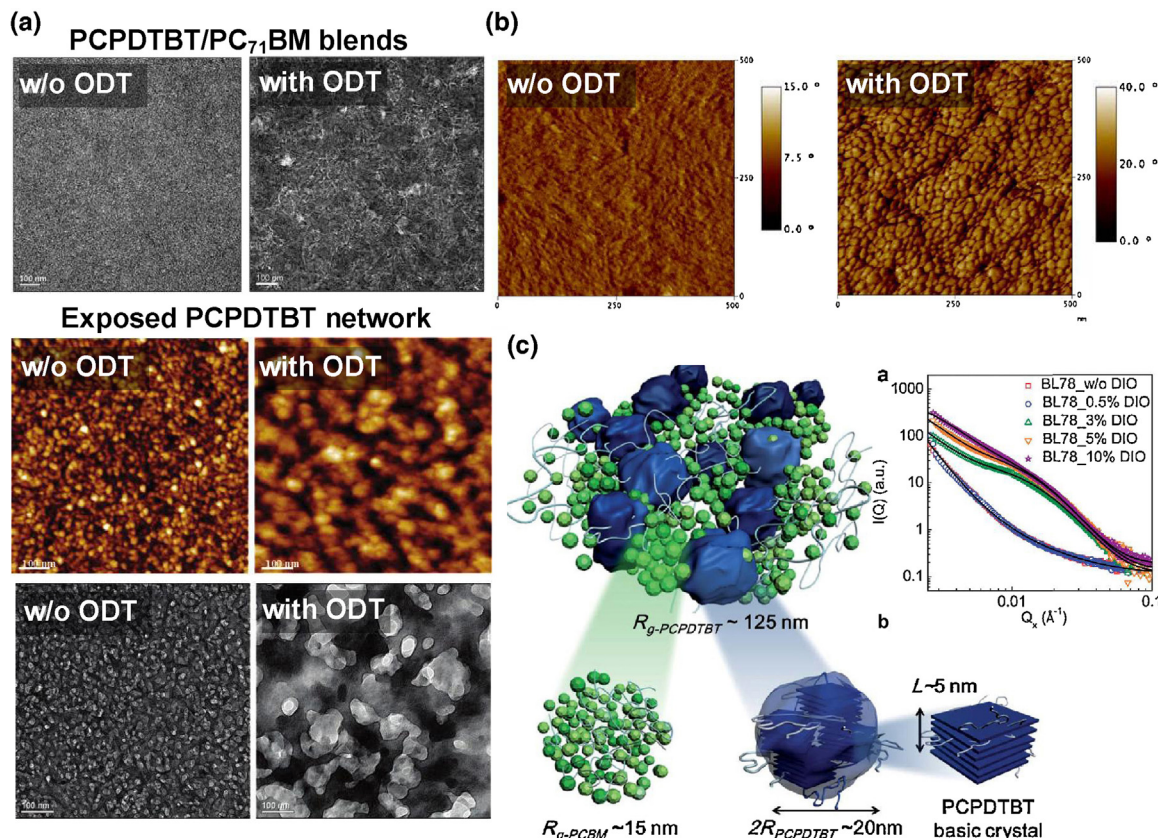


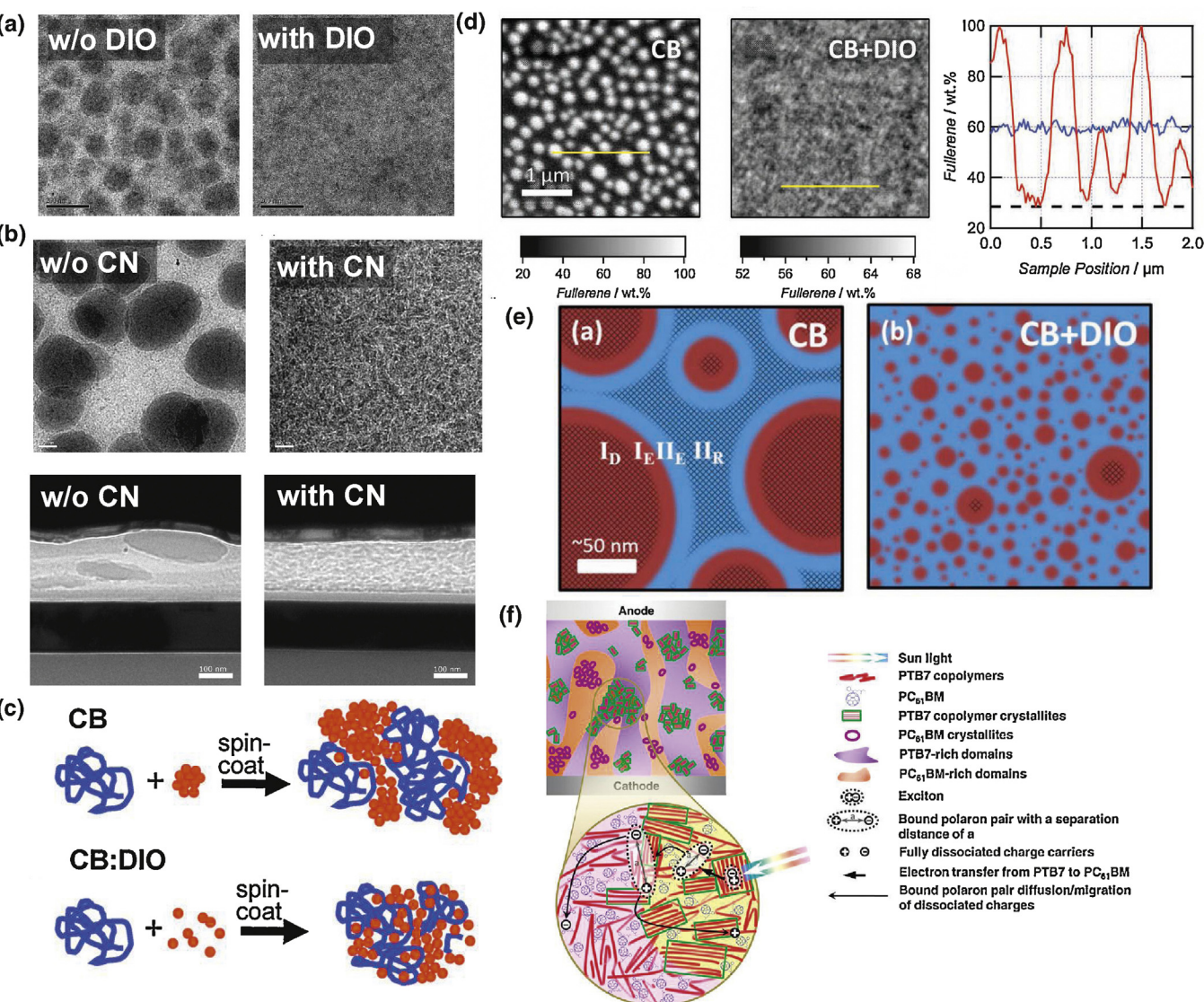
FIGURE 4

Examples of promoting phase separation by processing with solvent additives. (a) Top: TEM images of PCPDTBT/PC₇₁BM BHJ blends. Bottom: AFM and TEM images of exposed PCPDTBT networks from PCPDTBT/PC₇₁BM BHJs. (b) Phase images of PCPDTBT/PC₇₁BM BHJs. (c) Left: Illustration of the bi-hierarchical nanostructures of PCPDTBT/PC₇₁BM BHJs. Right: GISAXS profiles of PCPDTBT/PC₇₁BM BHJ processed with different amounts of additives. Reproduced with permission from [35,63,64]. © American Chemical Society, © Nature Publishing Group, © Royal Society.

characterization [7,62]. Similar to the additive effects on molecular organization, morphological variations of the phase-separated domains due to solvent additives also distinctively depend on the specific type of BHJ system under investigation. Nevertheless, rather than discussing each case by case, the morphological effects can be systematically categorized into either improving phase separation (type I) or suppressing oversized phase segregation (type II).

The blend of PCPDTBT/PC₇₁BM is a representative system of type I. Morphological variations affected by solvent additives were studied by Lee et al. [35]. AFM and TEM images (Fig. 4a) show homogeneous nanostructures with weak contrast of the PCPDTBT/PC₇₁BM film processed without DIO, suggesting strong inter-mixing of donors and acceptors at the molecular scale. In contrast, processing with the additive DIO promoted phase separation, which reveals larger-sized inter-connected regions of both PCPDTBT and PC₇₁BM components. Fibril-like domains

with strong contrast were observed in the TEM image (Fig. 4a). Moreover, after selectively removing the PC₇₁BM phase, both the TEM and AFM images exhibit phase-separated nanodomains (Fig. 4a). Higher resolution domains were observed in the phase images of AFM by Peet et al. as shown in Fig. 4b [63]. Evidence of spheroidal nanodomains in such DIO-assisted high-efficiency PCPDTBT/PC₇₁BM BHJ was provided in our previous work [64] employing the combination of GISAXS and GIWAXS techniques, Kelvin probe force microscopy (KPFM), and TEM to quantitatively demonstrate the bi-hierarchical nanostructures of both PCPDTBT and PC₇₁BM (Fig. 4c). Specifically, PCPDTBT networks formed by the aggregation of primary particles of several basic crystallites, and PC₇₁BM clusters aggregated from individual PC₇₁BM molecules. The effect of increasing the scale of phase-separation by additive processing was also revealed in other polymer/fullerene [46,48,65,66] and polymer/non-fullerene systems [67].

**FIGURE 5**

Examples of suppressing large-scaled phase segregation by solvent additives. (a) TEM images of PTB7/PC₇₁BM BHJs. (b) Top view and cross-section TEM images of Si-PDTBT/PC₇₁BM BHJs. (c) Schematics of PTB7/PC₇₁BM blends in solution and thin-film states. (d) Top: composition mapping of PTB7/PC₇₁BM BHJs and cross-section profiles. (e) Bottom: Schematic of PC₇₁BM domains (red) in PTB7/PC₇₁BM matrixes (blue). (f) Illustration of hierarchical nanostructure in PTB7/PC₇₁BM BHJ. Reproduced with permission from [54,56,68–70]. © American Chemical Society, © Wiley.

Type II effects of suppressing phase segregation are generally visually opposite to those of type I effects in microscopic observations. Liang et al. presented TEM images of PTB7/PC₇₁BM BHJ blends processed with a single host solvent revealing obvious large-scale phase segregation on the scale of hundreds of nanometers as shown in Fig. 5a [68]. Incorporating the additive DIO during spin coating effectively suppressed the formation of such segregation, which led to a more homogeneous nanomorphology (Fig. 5a). Similar nanostructural variations were extensively reported in other BHJ systems [36,69–75], as illustrated in Fig. 5b,c containing TEM observations [69] and schematic illustrations based on SAXS characterization [70]. Collins et al. quantitatively characterized the composition of phase-separated domains in PTB7/PC₇₁BM BHJ blends processed without and with additive DIO as shown in Fig. 5d [56]. The phase-separated domains having droplet shape were attributed to pristine PC₇₁BM embedded in the PTB7/PC₇₁BM matrixes with 70/30 weight ratio. Processing with additive DIO reduced the domain size from 177 nm to 34 nm (Fig. 5e), which was correlated with efficiency improvement larger than a factor of two. Interestingly, hierarchical nanostructure was

discovered in high-efficiency PTB7/PC₇₁BM BHJ blends, that is, crystallites of several nanometers, aggregations of crystallites spanning tens of nanometers, and networks constructed by polymer-rich and fullerene-rich domains approximately hundreds of nanometers in size (Fig. 5f) [54], which is similar to that observed in PCPDTBT/PC₇₁BM BHJ blends [64].

In both types, higher efficiency is correlated with a similar, hierarchical morphology. Intermixing or domain morphology should involve donor and acceptor species having average spacing smaller than ten nanometers to meet the criteria for efficient exciton dissociation, and the domain network structure should involve continuous pathways connected to the electrodes for efficient carrier transport. As proposed in our previous work, the opposite structural variations between the two types actually result from distinctive structures processed without additives, that is, inter-mixing in type I or large-scale segregation in type II. The intrinsic factors of miscibility, affinity, and thermodynamic equilibrium compositions between BHJ components as well as their tendency to crystallize may account for such differences [56,64].

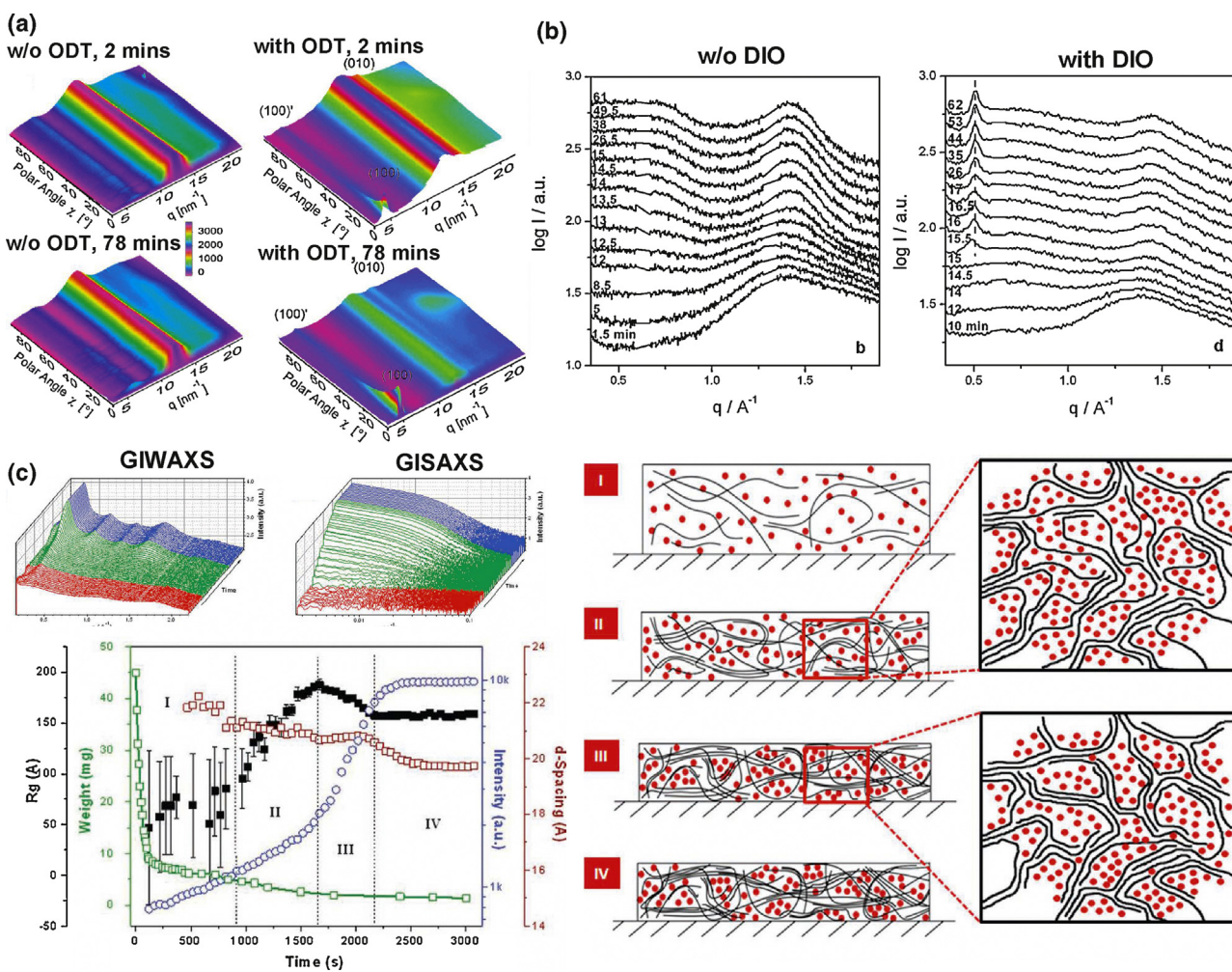


FIGURE 6

Examples of *in situ* characterization of BHJ blends during solvent drying. (a) 3D GIWAXS sector plots of PCDTBT/PC₇₁BM BHJs. (b) *In situ* GIWAXS profiles of PCDTBT/PC₇₁BM BHJs. (c) *In situ* GIWAXS and GISAXS profiles of pDPP polymer/PC₇₁BM BHJs with tracing plots shown below. The illustration of four-stage structural evolution according to the *in situ* GIWAXS/GISAXS results is shown on the right. Reproduced with permission from [36,52,76]. © American Chemical Society, © Wiley.

Structural evolution

Analysis of structural evolution of BHJ blends during solvent drying can be helpful for understanding the vital role of solvent additives in tuning BHJ nanostructures. Insights can be attained by utilizing powerful *in situ* characterization techniques. In the work presented by Rogers et al., PCPDTBT/PC₇₁BM BHJ films were *in situ* characterized using GIWAXS immediately after being spin coated (Fig. 6a) [52]. The enhanced diffraction from the (1 0 0) plane suggests that the additive ODT facilitates reducing the nucleation barrier of PCPDTBT, which organized into crystallites in the early stage of film formation (~2 min). Continuous nucleation and re-orientation of crystallites takes place during a prolonged solvent drying process (~78 min). For the same BHJ system, Gu et al. further employed GIWAXS to *in situ* characterize the structural evolution of drop-cast blends from solution state to solid state [76]. As presented in Fig. 6b, while the profiles of PCPDTBT/PC₇₁BM blend processed with the single solvent CB revealed only the form factor of PC₇₁BM around $q = 1.4 \text{ \AA}^{-1}$, additional scattering characteristics of PCPDTBT chain organization can be observed in the blend processed with the additive DIO. Namely, evolving from aggregated PCPDTBT chains in solution, swollen PCPDTBT chains with solvent, and finally the folded PCPDTBT chains in lamellar structures correspond to the $q = 0.65 \text{ \AA}^{-1}$, $q = 0.49 \text{ \AA}^{-1}$, $q = 0.51 \text{ \AA}^{-1}$, respectively. The authors hence interpreted that with the evaporation of CB, the residual CB/DIO gradually became a poorer solvent for PCPDTBT, which forced the chains to crystallize. Crystallites formed by this process effectively excluded the PC₇₁BM from intermixing, and the remaining PCPDTBT and PC₇₁BM were allowed to fill into the spaces between PCPDTBT crystallites.

Another example of quaterthiophene (pDPP)-based polymer/PC₇₁BM blends that can be grouped into type II BHJ systems was studied by Liu et al. using *in situ* GISAXS/GIWAXS techniques as shown in Fig. 6c [36]. It is worth noting that the DCB in the co-solvent of CF/DCB functions as solvent additive owing to its higher boiling point and selective solubility for PC₇₁BM. The authors proposed a four-stage BHJ structural evolution by tracing the residual solvent weight, domain size of heterojunction, scattering intensity, and lamellar spacing during solvent drying (Fig. 6c). In the early stages, most of the CF was gone, leading to aggregation of pDPP-based polymer in poor CF/DCB solvent and formation of crystal networks. With further solvent evaporation, the remaining polymer and PC₇₁BM were then deposited into the spaces left by the polymer aggregates. This evolution is similar to that of the PCPDTBT/PC₇₁BM case (type I) described above. Nevertheless, in some aspects they possess different functions: the construction of polymer aggregates/networks in the early stages forced by additive prevents the fullerene from segregating into oversized domains (hundreds of nanometers), whereas in the PCPDTBT/PC₇₁BM system the polymer aggregates (crystallites) formed early in the process prevent the fullerene from mixing into polymer aggregates.

Conclusions and future outlook

Controlling BHJ morphology is essential for achieving high PCE. Processing BHJ layers with solvent additives has proven to be an effective strategy toward achieving a nearly ideal BHJ morphology correlated with high efficiency. In this review, we

provided an overview of solvent additive effects on tuning BHJ morphology, starting from the selection of additive molecules to the BHJ morphological variations at local and global scales as well as their evolution during solvent drying. Interactions among BHJ components, host solvent, and additives are critical for achieving proper phase-separated domains with highly efficient exciton dissociation and carrier transport. The references reviewed herein are important resources for in-depth understanding of BHJ morphology control by solvent additive and can serve as the foundation for a rational guide to processing and materials design.

Practical application of organic photovoltaics will rely on high-throughput processing. However, virtually all device demonstration and fundamental research to date has utilized the spin coating process for thin film deposition. Such processing wastes a large amount of solution and is incompatible with large-scale processing and promising roll-to-roll fabrication. When employing other solution-based processing including slot-die coating, spray coating, screen printing, ink-jet printing, etc., the interplay among host solvent, additives, and BHJ materials as well as the resultant BHJ morphologies will surely be different from that based on spin coating. Further close cooperation between scientists and engineers is necessary to realize the large-scale production and commercialization toward a competitive technology.

Acknowledgement

Financial support obtained from the National Science of Council of Taiwan (101-3113-E-002-010) is highly appreciated. This work was performed, in part, at the Center for Nanoscale Materials, a U.S. Department of Energy, Office of Science, Office of Basic Energy Sciences User Facility under Contract no. DE-AC02-06CH11357.

References

- [1] G. Grancini, et al. *Nat. Mater.* 12 (2013) 29.
- [2] J. You, et al. *Nat. Commun.* 4 (2013) 1446.
- [3] Y.-J. Cheng, et al. *Chem. Rev.* 109 (11) (2009) 5868.
- [4] Y. Li, *Acc. Chem. Res.* 45 (5) (2012) 723.
- [5] L. Bian, et al. *Prog. Polym. Sci.* 37 (9) (2012) 1292.
- [6] C. Brabec, et al. *Chem. Soc. Rev.* 40 (3) (2011) 1185.
- [7] W. Chen, et al. *Energy Environ. Sci.* 5 (8) (2012) 8045.
- [8] M.A. Ruderer, P. Müller-Buschbaum, *Soft Matter* 7 (12) (2011) 5482.
- [9] M.A. Brady, et al. *Soft Matter* 7 (23) (2011) 11065.
- [10] F. Liu, et al. *J. Polym. Sci. Part B* 50 (15) (2012) 1018.
- [11] R.A. Janssen, J. Nelson, *Adv. Mater.* 25 (13) (2013) 1847.
- [12] S. Braun, et al. *Adv. Mater.* 21 (14–15) (2009) 1450.
- [13] C. Deibel, et al. *Adv. Mater.* 22 (37) (2010) 4097.
- [14] S. Sista, et al. *Energy Environ. Sci.* 4 (5) (2011) 1606.
- [15] Y.-W. Su, et al. *Mater. Today* 15 (12) (2012) 554.
- [16] O.V. Mikhenko, et al. *Energy Environ. Sci.* 5 (5) (2012) 6960.
- [17] W.L. Ma, et al. *Adv. Funct. Mater.* 15 (10) (2005) 1617.
- [18] G. Li, et al. *Nat. Mater.* 4 (11) (2005) 864.
- [19] Y. Kim, et al. *Nat. Mater.* 5 (3) (2006) 197.
- [20] X.N. Yang, et al. *Nano Lett.* 5 (4) (2005) 579.
- [21] G. Li, et al. *Adv. Funct. Mater.* 17 (10) (2007) 1636.
- [22] C.S. Kim, et al. *Adv. Mater.* 21 (30) (2009) 3110.
- [23] S.-H. Chan, et al. *Macromolecules* 44 (22) (2011) 8886.
- [24] K.R. Graham, et al. *Adv. Funct. Mater.* 5 (1) (2013) 63.
- [25] J.-F. Lin, et al. *J. Mater. Chem. A* 1 (3) (2013) 665.
- [26] S.Y. Chang, et al. *J. Mater. Chem. A* 1 (7) (2013) 2447.
- [27] C. Yang, et al. *J. Mater. Chem.* 19 (30) (2009) 5416.
- [28] J.-H. Tsai, et al. *Macromolecules* 43 (14) (2010) 6085.
- [29] H.C. Liao, et al. *ACS Nano* 6 (2) (2012) 1657.
- [30] J. Peet, et al. *Nat. Mater.* 6 (2007) 497.

- [31] Y.-M. Chang, L.-Y. Wang, *J. Phys. Chem. C* 112 (2008) 17716.
- [32] Y. Yao, et al., *Adv. Funct. Mater.* 18 (2008) 1783.
- [33] C. Yang, et al., *ACS Appl. Mater. Interfaces* 3 (10) (2011) 4053.
- [34] Y. Kim, et al., *Sol. Energy Mater. Sol. Cells* 105 (2012) 272.
- [35] J.K. Lee, et al., *J. Am. Chem. Soc.* 130 (2008) 3619.
- [36] F. Liu, et al., *Adv. Mater.* 24 (29) (2012) 3947.
- [37] M.M. Wienk, et al., *Adv. Mater.* 20 (13) (2008) 2556.
- [38] W. Li, et al., *J. Am. Chem. Soc.* 135 (15) (2013) 5529.
- [39] V.S. Gevaerts, et al., *Adv. Mater.* 24 (16) (2012) 2130.
- [40] C.M. Hansen, *Hansen Solubility Parameters: A User's Handbook*, CRC Press, Boca Raton, FL, 2000.
- [41] K.R. Graham, et al., *Adv. Funct. Mater.* 22 (22) (2012) 4801.
- [42] B. Walker, et al., *Adv. Energy. Mater* 1 (2) (2011) 221.
- [43] D.T. Duong, et al., *J. Polym. Sci. Part B* 50 (20) (2012) 1405.
- [44] J. Hildebrand, R.L. Scott, *The Solubility of Nonelectrolytes*, Reinhold, New York, 1950.
- [45] X. Liu, et al., *Adv. Mater.* 24 (5) (2012) 669.
- [46] H.-Y. Chen, et al., *J. Phys. Chem. C* 113 (18) (2009) 7946.
- [47] A.P.L. Böttiger, et al., *J. Mater. Chem.* 22 (42) (2012) 22501.
- [48] T. Salim, et al., *J. Mater. Chem.* 21 (1) (2011) 242.
- [49] Y. Sun, et al., *Adv. Energy. Mater* 1 (6) (2011) 1058.
- [50] X. Guo, et al., *Energy Environ. Sci.* 5 (7) (2012) 7943.
- [51] J.T. Rogers, et al., *Adv. Mater.* 23 (20) (2011) 2284.
- [52] J.T. Rogers, et al., *J. Am. Chem. Soc.* 134 (6) (2012) 2884.
- [53] Z. He, et al., *Nat. Photon.* 6 (2012) 591.
- [54] W. Chen, et al., *Nano Lett.* 11 (9) (2011) 3707.
- [55] M.R. Hammond, et al., *ACS Nano* 5 (10) (2011) 8248.
- [56] B.A. Collins, et al., *Adv. Energy Mater.* 3 (1) (2013) 65.
- [57] D.H. Kim, et al., *Chem. Mater.* 25 (3) (2013) 431.
- [58] V.D. Mihaletechi, et al., *Adv. Funct. Mater.* 16 (5) (2006) 699.
- [59] T. Erb, et al., *Adv. Funct. Mater.* 15 (7) (2005) 1193.
- [60] L. Ye, et al., *Adv. Mater.* 24 (47) (2012) 6335.
- [61] Y.-C. Huang, et al., *J. Phys. Chem. C* 116 (18) (2012) 10238.
- [62] J. Rivnay, et al., *Chem. Rev.* 112 (10) (2012) 5488.
- [63] J. Peet, et al., *Nat. Mater.* 6 (7) (2007) 497.
- [64] H.-C. Liao, et al., *Energy Environ. Sci.* 6 (6) (2013) 1938.
- [65] J. Yuan, et al., *Adv. Funct. Mater.* 23 (7) (2013) 885.
- [66] A.J. Moule, K. Meerholz, *Adv. Mater.* 20 (2) (2008) 240.
- [67] G. Ren, et al., *Adv. Energy Mater.* 1 (5) (2011) 946.
- [68] Y. Liang, et al., *Adv. Mater.* 22 (20) (2010) E135.
- [69] J.S. Moon, et al., *Nano Lett.* 10 (10) (2010) 4005.
- [70] S.J. Lou, et al., *J. Am. Chem. Soc.* 133 (51) (2011) 20661.
- [71] J. Jo, et al., *Adv. Energy Mater.* 2 (11) (2012) 1397.
- [72] S. Kwon, et al., *Adv. Energy Mater.* 2 (12) (2012) 1420.
- [73] M.S. Su, et al., *Adv. Mater.* 23 (29) (2011) 3315.
- [74] J. Min, et al., *Chem. Mater.* 24 (16) (2012) 3247.
- [75] E. Zhou, et al., *Energy Environ. Sci.* 5 (12) (2012) 9756.
- [76] Y. Gu, et al., *Adv. Energy Mater.* 2 (6) (2012) 683.
- [77] Z. He, et al., *Adv. Mater.* 23 (40) (2011) 4636.
- [78] H. Zhou, et al., *Adv. Mater.* 23 (11) (2013) 1646.
- [79] S.M. Yoon, et al., *Nano Lett.* 12 (12) (2012) 6315.
- [80] L. Huo, et al., *Angew. Chem. Int. Ed.* 50 (41) (2011) 9697.
- [81] X. Li, et al., *Adv. Mater.* 24 (22) (2012) 3046.
- [82] S. Chen, et al., *Adv. Energy Mater.* 2 (11) (2012) 1333.
- [83] C.M. Amb, et al., *J. Am. Chem. Soc.* 133 (26) (2011) 10062.
- [84] C.E. Small, et al., *Nat. Photon.* 6 (2011) 115.
- [85] B.R. Aich, et al., *Org. Electron.* 13 (9) (2012) 1736.
- [86] E.T. Hoke, et al., *Adv. Energy Mater.* 3 (2) (2013) 220.
- [87] C. Cabanatos, et al., *J. Am. Chem. Soc.* 135 (12) (2013) 4656.
- [88] T. Yang, et al., *Energy Environ. Sci.* 5 (8) (2012) 8208.
- [89] H.-Y. Chen, et al., *Nat. Photon.* 3 (2009) 649.
- [90] X. Yang, et al., *Adv. Energy Mater.* 3 (5) (2013) 666.
- [91] Z. Tan, et al., *Adv. Mater.* 24 (11) (2012) 1476.
- [92] T.Y. Chu, et al., *J. Am. Chem. Soc.* 133 (12) (2011) 4250.
- [93] C.Y. Chang, et al., *Angew. Chem. Int. Ed.* 50 (40) (2011) 9386.
- [94] H. Zhou, et al., *Angew. Chem. Int. Ed.* 50 (13) (2011) 2995.
- [95] S.C. Price, et al., *J. Am. Chem. Soc.* 133 (12) (2011) 4625.
- [96] L. Yang, et al., *J. Am. Chem. Soc.* 134 (12) (2012) 5432.
- [97] C.Y. Chang, et al., *Adv. Mater.* 24 (4) (2012) 549.
- [98] C.J. Takacs, et al., *J. Am. Chem. Soc.* 134 (40) (2012) 16597.
- [99] L. Dou, et al., *Nat. Photon.* 6 (2012) 180.
- [100] L. Dou, et al., *J. Am. Chem. Soc.* 134 (24) (2012) 10071.
- [101] J. Yang, et al., *Adv. Mater.* 23 (30) (2011) 3465.
- [102] Y. Kim, et al., *Energy Environ. Sci.* 6 (6) (2013) 1909.
- [103] C. Piliego, et al., *J. Am. Chem. Soc.* 132 (2010) 7595.
- [104] S.B. Darling, F. You, *RSC Adv.* (2013), <http://dx.doi.org/10.1039/C3RA42989J>.